PCCP

Accepted Manuscript

ROYAL SOCIETY OF CHEMISTRY

www.rsc.org/pccp

Vibronic energy relaxation approach highlighting deactivation pathways in carotenoids†

Vytautas Balevičius Jr.,[a] Arpa Galestian Pour,[b] Janne Savolainen,[c] Craig N. Lincoln,[b] Vladimir Lukes,[d] Eberhard Riedle,[e] Leonas Valkunas,[a,f] Darius Abramavicius[a] and Jürgen Hauer*[b]

Received Xth XXXXXXXXXX 20XX, Accepted Xth XXXXXXXXX 20XX
First published on the web Xth XXXXXXXXXX 200X **DOI: 10.1039/b000000x**

Energy relaxation between two electronic states of a molecule is mediated by a set of relevant vibrational states. We describe this fundamental process in a fully quantum mechanical framework based on first principles. This approach explains population transfer rates as well as describes the entire transient absorption signal as vibronic transitions between electronic states. By applying this vibronic energy relaxation approach to carotenoids, we show that β-carotene's transient absorption signal can be understood without invoking the intensely debated S^* electronic state. For a carotenoid with longer chain length, we find that vibronic energy relaxation does not suffice to explain all features in the transient absorption spectra, which we relate to an increased ground state structural inhomogeneity. Our modeling approach is generally applicable to photophysical deactivation processes in molecules. As such, it represents a well-founded alternative to data fitting techniques such as global target analysis.

1 Introduction

In large organic molecules, ultrafast energy transfer between two electronic states is mediated by nuclear motions[1]. Carotenoids present a biologically important case of such vibronic energy relaxation. Their optical properties are defined by the π-conjugated electronic states, extended along the polyene backbone as depicted in Fig. 1. The earliest suggested energy flow models used a three-level system with ground state S_0 and excited states S_2 and S_1[2]. The linear absorption spectra of carotenoids stem from transitions between the electronic ground state S_0 and the "bright" electronic excited state S_2, whereas the lowest-lying excited state S_1 is "dark", with the $S_0 \rightarrow S_1$ transition being one-photon forbidden. The properties of S_1 are observed either by two-photon absorption from S_0 or by using nonlinear transient absorption (TA) spectroscopy. In TA spectroscopy, two ultrashort pulses interact with the investigated sample: first with the excitation pulse called pump-pulse, followed by a probe pulse that records the evolving transient spectra as a function of delay time t. In TA spectra of carotenoids, a characteristic excited state absorption (ESA) band from S_1 to higher-energy states ($S_1 \rightarrow S_n$) is readily detected due to its strong transition dipole moment[2]. Already through the early spectrally resolved TA experiments it became evident that a mere 3-level picture is inadequate in describing the observed transient spectra in detail[3]. The main discrepancy between the 3-level model and the observed transient spectra concerns the so-called S^* feature. S^* manifests itself spectrally as a high-energy shoulder of the ESA from S_1 and has a slightly longer lifetime than S_1, depending on the chain length of the investigated carotenoid[4]. To date, the consensus over the details of carotenoid deactivation pathways is still lacking and the origin of the S^* feature is a subject of continuing debate, as reviewed by Polivka and Sundström[2,4]. This is mainly because none of the proposed models are able to account for all the reported experimental observations.

In the early studies using TA measurements, S^* was interpreted as an electronically excited state situated in the vicinity of S_1 and drawing population from the same initially excited state S_2. It was proposed that S^* subsequently delivers population to the bacteriochlorophylls in photosynthetic complexes[5] and also serves as a triplet-precursor state in spirilloxanthin[3] (the latter point has been drawn into question recently[6,7]). However, sequential energy flow models[8], where S^* is populated after S_1, fail to explain the pump–deplete–probe experiments[9], where S_2 is depleted by a pulse in the near-infrared. It was observed that only S_1 and not S^* is affected, which should not be the case if S_2 is a common precursor for both S_1 and S^*. The pump–deplete–probe experiments seemed to

† Electronic Supplementary Information (ESI) available: see DOI: 10.1039/b000000x/

[a] *Department of Theoretical Physics, Faculty of Physics, Vilnius University, Sauletekio Ave. 9, build. 3, LT-10222 Vilnius, Lithuania*
[b] *Photonics Institute, Vienna University of Technology, Gusshausstrasse 27, 1040 Vienna, Austria*
[c] *Department of Physical Chemistry II, Ruhr-University Bochum, 44780 Bochum, Germany*
[d] *Department of Chemical Physics, Slovak University of Technology, Radlinského 9, 81237 Bratislava, Slovakia*
[e] *Lehrstuhl für BioMolekulare Optik, Ludwig-Maximilians-University, Oettingenstrasse 67, 80538 Munich, Germany*
[f] *Center for Physical Sciences and Technology, Institute of Physics, Savanoriu Ave. 231, LT-02300 Vilnius, Lithuania*
* E-mail: juergen.hauer@tuwien.ac.at

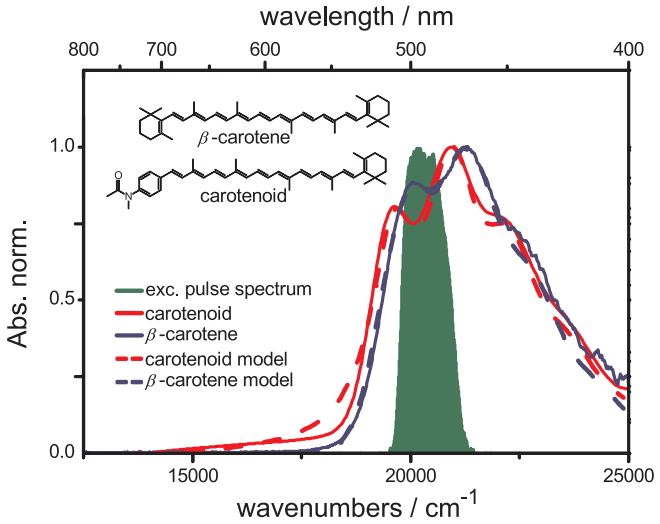

Fig. 1 The absorption spectra of β-carotene in benzonitrile (red line) and the derivative carotenoid in toluene (blue line), and their molecular structures. Solid lines show the measured data and dashed lines correspond to the simulation. The excitation pulse is shown in green.

support the preexisting hypothesis of S^* as a vibrationally hot ground state[10], populated by either Impulsive Stimulated Raman Scattering (ISRS)[9,11] or nonradiatively populated from S_1[8,10,12]. However, the hot ground state hypothesis was ruled out by ISRS experiments using narrow band excitation, which should have prevented the formation of hot-S_0[13]. An additional argument against hot-S_0 based on theoretical considerations was brought forth by Christensson *et al.*[14], who showed that hot-S_0 fails to predict the correct sign of the ESA signal associated with S^*.

Alternatively, S^* was also interpreted as a signal from S_1 after excited state isomerization[15]. While explaining the 200 fs build-up dynamics and sign of S^* correctly, the temperature dependence of the S_1/S^* ratio raises further questions. As shown in previous works, S^* can be "frozen out", meaning that the S^* features lose amplitude upon cooling[16–18]. The femtosecond isomerization timescale, however, speaks against the thermally activated build-up process. Further, Holzwarth and co-workers proposed that the photodynamics of β-carotene could be satisfactorily explained by a sequential model, i.e., $S_2 \rightarrow S_{1\nu} \rightarrow S_{1\nu'} \rightarrow S_0$, where $S_{1\nu}$ and $S_{1\nu'}$ are two vibrationally excited states of the S_1 potential energy surface, without involvement of S^*[19]. No signatures of S^* in β-carotene were observed by Holzwarth and co-workers and contradicting findings in other studies were attributed to sample impurities, although other groups observed S^* features in purified samples of various carotenoids including β-carotene[17]. Recently, the product of different ground state conformers were suggested to explain the S^* features[14,20,21]. In this case, the role of the end groups of carotenoids was re-evaluated within the so-called inhomogeneous ground state model, showing that conformers with different dihedral angles between the end group and the near-planar polyene chain have energy differences between their respective thermally populated energetic minima.

The difficulties in the assignment of the S^*-related features in TA stem from the strong overlap between the ESA of S_1 and S^*. This leads to ambiguities in a wide-spread data analysis approach called global target analysis (GTA) brought about by Holzwarth[22]. In GTA a complex quantum mechanical molecular system is described by a set of states, or configurations, and the dynamics of the state populations are described by a simple master equation. In other words, GTA does not require any physical, microscopic picture of the studied system. The great appeal of GTA is thus easy to understand: it can readily describe spectrally broad TA data sets, which often pose an analysis challenge. To this end, GTA is a model testing approach: the correctness of the postulated kinetic energy level scheme (often based on intuition and/or knowledge from other experiments) is then determined by the χ^2 at convergence of the fitting procedure. In the case of similar time constants and overlapping spectral features, GTA cannot give a unique solution, *i.e.*, more than one target model and even more than one solution to one target model can give comparable χ^2 at convergence[23]. Furthermore, the GTA approach is essentially a multi-exponential fit. If the resolved time constants are closer to each other than one order of magnitude, they lose their meaning as they become increasingly coupled. In the case of the S^*-problem any multi-exponential solution falls into this regime of not well defined exponential terms. Finally, an important aspect of GTA is its inherent assumption that the data is separable into time and frequency dependent components (see ESI for details[†]). Dynamical spectral features such as the Stokes shift[24] or vibrational cooling[19] violate this basic assumption. Due to the generality of the approach, GTA will still fit experimental data satisfactorily in these cases, yet the retrieved time constants and spectral shapes will not necessarily reflect real physical behavior.

In this work, we present a multi-step vibrational cooling model of the carotenoid states. We formalize it using quantum relaxation theory[25,26], and include the known electronic states and two strongest vibrational modes in the system Hamiltonian. This approach provides a unified treatment of spectral lineshapes and population dynamics and hence avoids the ambiguities associated with GTA described above. In literature, the vibrational relaxation in carotenoids is described by kinetic schemes involving a single abstract state hot-S_1[7,10], or a cascade of several vibrationally excited states[19,27–29]. Here, we consider the S_1 state as a manifold of vibrational states by explicitly including symmetric carbon–carbon single and double bond stretching modes. Furthermore, it is known that the characteristic vibrational structure of the absorption spec-

tra of carotenoids (Fig. 1) originates from transitions to the lowest vibrational levels of the S_2 state, which in turn are the combination of the aforementioned C=C and C–C stretching modes[2]. Accordingly, we assume that the ESA from S_1 to S_n is also governed by a similar vibronic progression involving these two modes. The resulting model has four states (S_0, S_1, S_2, S_n, see Fig. 2) to describe the time-resolved excitation dynamics within carotenoids. As will be shown, this vibrational cooling model reproduces the experiments on β-carotene with high accuracy. Additionally, we apply our theory to 7-apo-7-(4-aminophenyl)-β-carotene, a β-carotene derivative[30] further referred to simply as the carotenoid, in which one of the two β-ionyliden endgroups is replaced with a phenyl ring (Fig. 1). For this molecule, the vibrational cooling on the S_1 state is not sufficient to explain the observed kinetics, especially at long delays in the spectral region associated with the S^* state. However, we show how the carotenoid, in contrast to β-carotene, has an increased structural inhomogeneity in its ground-state and consequently the inhomogeneous ground state model[20,21] provides the physical basis for the observed S^*-related features.

2 Vibronic Energy Relaxation Approach (VERA)

During ultrafast internal conversion the energy difference between the electronic states is completely converted into vibrational excess energy. In contrast to the widely used phenomenological approaches, VERA derives population transfer rates using quantum relaxation theory. The energy transfer is induced by the low-frequency intra- and intermolecular phonon modes. The high-frequency vibrational modes act as a reservoir for the temporary storage of the excess energy and may determine the line shapes of transitions via their corresponding Franck–Condon (FC) factors.

For an adequate description of a carotenoid, we consider four electronic states $|i\rangle \equiv |S_0\rangle, |S_1\rangle, |S_2\rangle, |S_n\rangle$ with two high-frequency harmonic vibrational coordinates coupled to the electronic transitions. The vibrational modes are quantized, thus each electronic state $|i\rangle$ corresponds to a manifold of vibrational states $|i\rangle \equiv |a_i\rangle|b_i\rangle$. Index a indicates the number of quanta of the C=C stretching mode, having the frequency $\varepsilon_\alpha = 1522\,\mathrm{cm}^{-1}$ (we use $\hbar = 1$), and index b corresponds to the C–C mode with frequency $\varepsilon_\beta = 1156\,\mathrm{cm}^{-1}$. In the Condon approximation, each transition between arbitrary electronic states is accompanied by a "vertical" transition between vibrational states. Hence, in our model all the elementary transitions from i to j are characterized by the spectral line-shape $\sigma_\mathrm{X}(\omega)$ (*e.g.*, Gaussian or Lorentzian) multiplied by the electronic transition dipole moment μ_{ij} and the vibrational FC overlap integrals $\langle a_i|a'_j\rangle$, $\langle b_i|b'_j\rangle$.

The absorption spectrum of the carotenoid is given by the optically allowed $S_0 \to S_2$ electronic transition. As the vibrational frequencies are higher than the thermal energy, only the zero-quanta state $|a_{S_0}\rangle|b_{S_0}\rangle = |0_{S_0}\rangle|0_{S_0}\rangle$ is occupied in the equilibrium. The absorption spectrum is then given by

$$I_\mathrm{A}(\omega) = \sum_{a'b'} |\mu_{02}|^2 \langle 0_{S_0}|a'_{S_2}\rangle^2 \langle 0_{S_0}|b'_{S_2}\rangle^2 \sigma_\mathrm{A}(\omega - \omega^{(20)} - \omega_{00,a'b'}; \Delta\omega_\mathrm{A}), \quad (1)$$

where $\omega^{(20)}$ is the electronic energy gap between $|S_0\rangle$ and $|S_2\rangle$, $\omega_{ab,a'b'} = \varepsilon_\alpha(a'_j - a_i) + \varepsilon_\beta(b'_j - b_i)$ is the energy gap between the vibrational levels ab and $a'b'$, and $\Delta\omega_\mathrm{A}$ is the width of the line-shape. The FC overlaps are determined by displacements $d_\alpha^{(20)}$, $d_\beta^{(20)}$ between the minima of the electronic states' potentials[26], as shown in Fig. 2.

A simplified third-order nonlinear response function approach is considered to describe the TA spectra[25,26]. Therein only *incoherent* excitation dynamics are taken into account, which is justified as long as the electronic coherence decay is faster than the time between optical interactions. This holds for the TA spectroscopy when the delay times between the pulses exceed the used pulse widths (here $\sim$ 50-100 fs). Four interactions with the optical field are included: the first and second with the field of the pump-pulse, the third with the field of the probe-pulse and the last one determines the emitted field, which interferes with the transmitted probe-field. The time delays between the system–field interactions describe specific processes: the first delay is associated with the absorption line-shape which scales the absorption intensity of the pump-pulse, the second delay coincides with the delay between the pump- and the probe-pulses, while the third delay describes the line-shape of the detected spectrum. The TA spectrum is then given by a superposition of three interaction configurations denoted by stimulated emission (SE), ground state bleach (GSB) and ESA[25,26]:

$$\Delta A(\omega,t) = A_\mathrm{ESA}(\omega,t) - A_\mathrm{GSB}(\omega,t) - A_\mathrm{SE}(\omega,t), \quad (2)$$

where the three terms correspond to various transitions between system states (the states of a carotenoid are defined in Fig. 2). In the incoherent regime each of the three terms has the generic form

$$A_\mathrm{X}(\omega,t) = \sum_i I_{i(\mathrm{X})}(\omega) n_i(t) \quad (3)$$

with $\mathrm{X} = \mathrm{ESA}, \mathrm{GSB}, \mathrm{SE}$, $n_i(t)$ denote the populations of the states i from which the transition takes place for the specific process X, and $I_{i(\mathrm{X})}(\omega)$ is the corresponding line-shape. The four electronic states of carotenoids participate in these processes as follows: $S_0 \to S_2$ is responsible for the absorption and for GSB. Consequently $S_2 \to S_0$ gives SE. The S_1 state

is obtained by nonradiative relaxation $S_2 \rightarrow S_1$; state S_n is involved in the optical $S_1 \rightarrow S_n$ transition corresponding to ESA. We note that ESA from S_2 is possible but is only present during the ultrashort (sub-100 fs) lifetime of S_2 and, therefore, is omitted in our model consideration[31]. A spectrum for the specific process in TA is given similarly to the absorption:

$$I_{i(\mathrm{X})}(\omega) = \sum_{ja'b'ab} |\mu_{ij}|^2 \langle a_i|a'_j\rangle^2 \langle b_i|b'_j\rangle^2 \sigma_{\mathrm{X}}(\omega - \omega_{\mathrm{X}} - \omega_{ab,a'b'}; \Delta\omega_{\mathrm{X}}). \quad (4)$$

Here, ω_{X} and $\Delta\omega_{\mathrm{X}}$ are the electronic energy gap and the full width at the half maximum (FWHM) of a transition in X configuration, respectively.

Each spectral component $A_{\mathrm{X}}(\omega,t)$ can then be given by considering the scheme presented in Fig. 2. When X=GSB, the signal is represented as a missing (negative) absorption. For X=SE we make an assumption that at short delay times the emission line-shape is a mirror image of the absorption red-shifted by the Stokes shift $\delta\omega_{\mathrm{St.}}$ that renormalizes the central emission frequency $\omega_{\mathrm{SE}} = \omega^{(20)} - \delta\omega_{\mathrm{St.}}$. The initial state is then the time-dependent vibrationally relaxed S_2 state, $|a_i\rangle|b_i\rangle = |0_{S_2}\rangle|0_{S_2}\rangle$. In the case of X=ESA, we assume, that the transitions can take place from an arbitrary vibrational state of S_1, to all vibrational states of S_n with the electronic energy gap $\omega_{\mathrm{ESA}} = \omega^{(n1)}$ while the FC factors are governed by the displacements $d_\alpha^{(n1)}$, $d_\beta^{(n1)}$ (*conf.*, Fig. 2).

To model the excited state population dynamics $n_i(t)$, we derive the equations of motion for the density matrix based on the Hamiltonian of two electronic states, S_2 and S_1, represented by harmonic oscillators on shifted potential energy surfaces. The non-radiative transitions between the states originate from phonon-induced off diagonal fluctuations characterized by two bath spectral densities $C_c''(\omega)$ and $C_f''(\omega)$. The former describes the fluctuations affecting the coordinates of the C=C and C–C oscillators of the system, and hence characterizes the vibrational relaxation. The latter describes the fluctuations, which induce the coupling between the electronic states S_1 and S_2, hence characterizing the internal conversion. Parametrization of both spectral densities is obtained by choosing the Drude spectral density, which is a semi-classical model describing the classical bath at high temperature[25]:

$$C''_{c/f}(\omega) = 2\lambda_{c/f}\frac{\omega\gamma}{\omega^2+\gamma^2}. \quad (5)$$

It is parametrized by the reorganization energies λ_c and λ_f and the relaxation rate γ. The same functional form for both spectral densities $C''_{c/f}(\omega)$ is assumed due to the same promoting phonon modes of the bath in the two processes. The resultant equations of motion are given in the ESI†.

We evaluate the parameters of our approach by fitting β-carotene and carotenoid TA data. To ensure that both

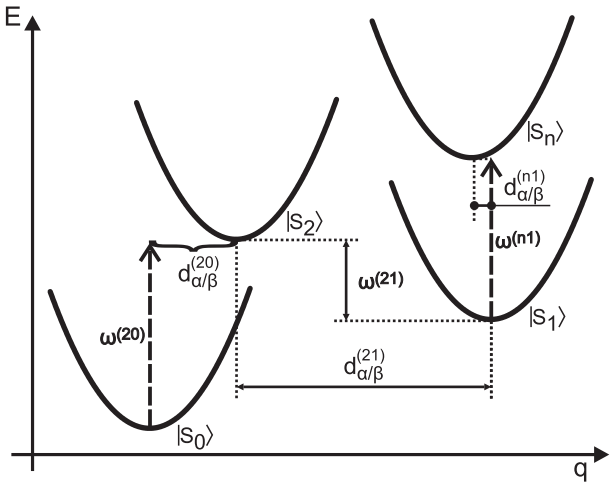

Fig. 2 Representation of the electronic states of a carotenoid as mutually shifted potential energy surfaces. The four states of the model, $|S_0\rangle, |S_1\rangle, |S_2\rangle, |S_n\rangle$, are shown. $\omega^{(ij)}$ denote the energy gaps between the states j and i; $d_{\alpha/\beta}^{(ij)}$ denote the displacements along the respective coordinate (α/β) between the potential minima of the states j and i.

static and dynamical system properties are accurately described, we first divide the parameters into two groups: the ones responsible for the spectral shapes ("static parameters": $\omega^{(20)}$, $\omega^{(n1)}$, $\Delta\omega_{\mathrm{GSB}} = \Delta\omega_{\mathrm{SE}}$, $\Delta\omega_{\mathrm{ESA}}$, $d_{\alpha/\beta}^{(20)}$, $d_{\alpha/\beta}^{(n1)}$, $\delta\omega_{\mathrm{St.}}$) and the others that describe the relaxation dynamics ("dynamic parameters": $\omega^{(21)}$, $d_{\alpha/\beta}^{(21)}$, $\lambda_{c/f}$, γ). The static parameters (see Table S1 in the ESI†) are determined by fitting the line-shapes of the linear absorption spectrum and the TA spectra at long times when population is fully relaxed in the vibrational manifold of S_1. To demonstrate the quality of the fit, the simulated absorption spectra of β-carotene and the carotenoid are shown together with the experimental spectra in Fig. 1. The excellent agreement also confirms that already the two high-frequency vibrational modes considered are sufficient for an effective description of the system.

Finding the correct dynamical parameters is less straightforward as the model includes two relaxation processes: the excitation transfer between electronic states $S_2 \rightarrow S_1$ and the subsequent vibrational relaxation within the S_1 manifold. The overall rate of the transition between the electronic states depends on the spectral density $C_f''(\omega)$ and the FC factors. The values for the energy gap and the displacements $d_{\alpha/\beta}^{(21)}$ can be taken from experiments to some accuracy. We have therefore considered the reported values of the gap $\omega^{(21)}$, the S_2 lifetime and vibrational relaxation[2] to determine the starting values of $\lambda_{c/f}$ and γ. The final consistent set was then obtained by fitting all the measured TA spectra at different time delays. The fitting was performed by means of visual comparison and

not a numerical algorithm. The procedures are described in the ESI† in greater detail. We find that both the carotenoid and β-carotene data is characterized by the following values $\omega^{(21)} = 6450\,\mathrm{cm}^{-1}$, $d_\alpha^{(21)} = d_\beta^{(21)} = 1.0$, $\lambda_c = 170\,\mathrm{cm}^{-1}$. The inducing low frequency intra- and intermolecular phonon modes are represented by the spectral density, Eq. (5), which peaks at $\approx 32\,\mathrm{cm}^{-1}$, corresponding to the damping parameter $\gamma = 164\,\mathrm{fs}$. An essential difference between the two samples is observed in λ_f, which is $\lambda_f^{\mathrm{car}} = 390\,\mathrm{cm}^{-1}$ for the carotenoid and $\lambda_f^{\beta-\mathrm{car}} = 480\,\mathrm{cm}^{-1}$ for β-carotene. In addition, we find the following Stokes shift values necessary for a satisfactory fit: $\delta\omega_{\mathrm{St.}}^{\mathrm{car}} = 100\,\mathrm{cm}^{-1}$, $\delta\omega_{\mathrm{St.}}^{\beta-\mathrm{car}} = 400\,\mathrm{cm}^{-1}$. We note that the values for $\omega^{(21)}$ and $d_{\alpha/\beta}^{(21)}$ are of the same order as those previously reported[2,32], and such consistency allows us to conclude that the values of the dynamical parameters are reasonable.

3 Results

The experimental TA spectra of β-carotene and the carotenoid are shown in Figs. 3(a) and 4(a), respectively. Both samples exhibit similar broad features of negative GSB above $\sim 19000\,\mathrm{cm}^{-1}$ and positive ESA at lower frequencies. Temporal cuts at chosen probe delays are shown in Figs. 3 and 4 separately for early times (panels (b)) and later times (panels (c)). Solid lines depict the experimental spectra, while simulated data are represented by the dashed lines. All data sets are normalized at the temporal and spectral maxima of the positive ESA signals. For both, β-carotene and the carotenoid, the GSB signal has the vibronic progression of the corresponding linear absorption spectrum. Also, the respective ESA signals bear resemblance as they both show a strong positive peak around $16500\,\mathrm{cm}^{-1}$. The ESA features are further accompanied by a blue-shifted shoulder, which is more pronounced in the carotenoids case, as can be seen when comparing the panels (b) and (c) of Fig. 3 with the ones of Fig. 4. This shoulder coincides with the controversially discussed S^* signal.

The overall spectral evolution of ESA comprises of the spectral narrowing and blue-shift of the initial peak. These features stem from the vibrational cooling in the S_1 state and are characteristic to the TA spectra of carotenoids[33,34]. It is interesting to note that the blue-shift for β-carotene is only tens of reciprocal centimeters (Fig. 3(b)), whereas it is of several hundreds of reciprocal centimeters for the carotenoid (Fig. 4(b)). In order to account for the large blue-shift in the carotenoid data, we additionally introduced reorganization dynamics by allowing the ESA central frequency $\omega_{\mathrm{ESA}}(t)$ to relax exponentially ($\omega_{\mathrm{ESA}}(t) = \omega_{\mathrm{ESA}}(0) - 800\exp(-t/\tau)$ [cm^{-1}] with $\tau = 200\,\mathrm{fs}$). Nevertheless, even with the added blue-shift, the simulations differ slightly from the experimental data in the very early $t < 200\,\mathrm{fs}$ time window (panels (b) in

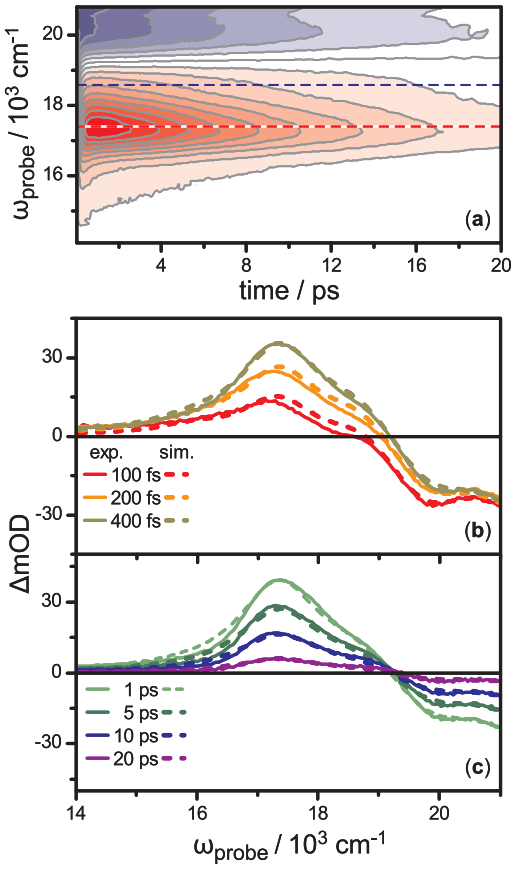

Fig. 3 Experimental TA data of β-carotene in (a). Positive (negative) signals are shown in red (blue) colours. Contour lines are drawn in 10% steps. Experimental (exp., solid lines) vs. simulation (sim., dashed) data at indicated pump–probe delay times for early (b) and late (c) values.

Figs. 3 and 4). These discrepancies can have several origins. For instance, the $S_2 \rightarrow S_{n(2)}$ ESA contribution, known to be present at $\sim 17000\,\mathrm{cm}^{-1}$ [20,31], is not included in the model. Further contributions stem from pulse overlap effects, which raise coherent interaction configurations[25,35,36] omitted in the present approach. Thus, although the experimental data in the sub-200 fs window show rich features they are excluded in the discussion below.

Based on the temporal cuts shown in panels (b) and (c) of Figs. 3 and 4, S^* and the other features are, to a large extent, well described and reproduced in the simulated data. However, when plotting slices along the pump–probe delay at specific detection frequencies, the differences between simulated and experimental results as well as between the samples become more apparent. These spectral cuts are shown in Fig. 5. When comparing simulated and measured kinetics at the S_1-maximum in the case of β-carotene (Fig. 5(a)), it is evident

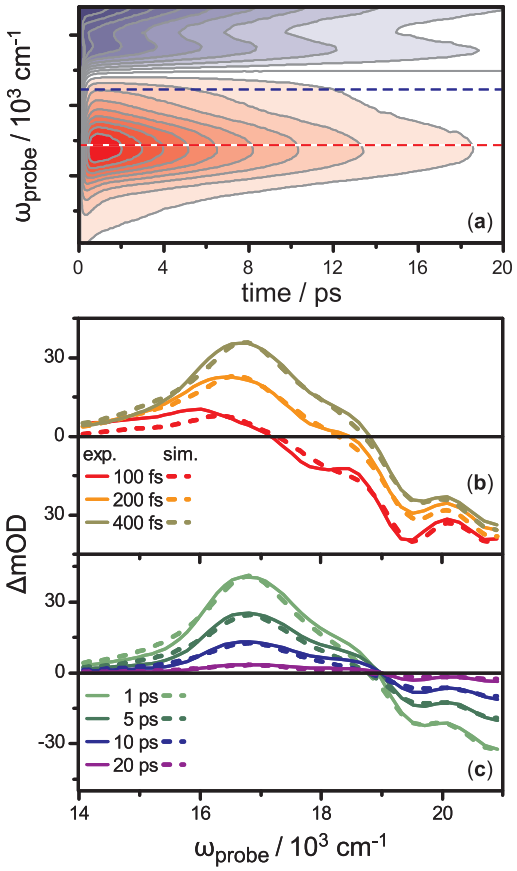

Fig. 4 Experimental TA data for the carotenoid in (a). Positive (negative) signals are shown in red (blue) colours. Contour lines are drawn in 10% steps. Experimental (exp., solid lines) vs. simulation (sim., dashed) data at indicated pump–probe delay times for early (b) and late (c) values.

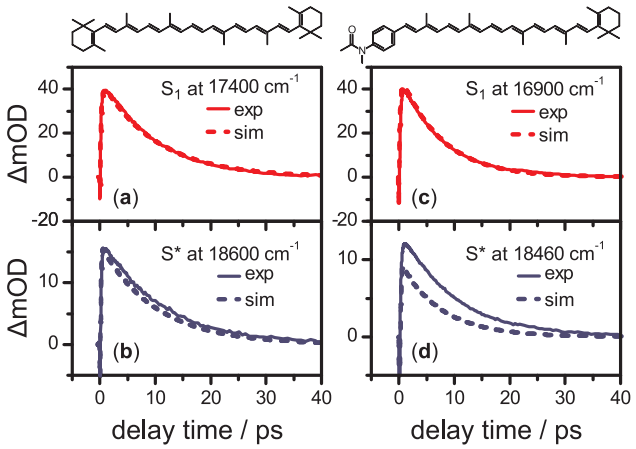

Fig. 5 Kinetic traces for β-carotene (left column) and the carotenoid (right column) for S_1- (red lines) and the S^*-specific detection energies (blue lines), as indicated by horizontal lines in Figs. 2 and 3. Solid lines correspond to the experimental results, whereas dashed lines indicate simulations.

that our model reproduces the observed dynamics well. At the S^*-maximum, with time traces shown in Fig. 5(b), the match is still very good, illustrating the point that an in depth treatment of vibrational cooling on S_1 as done here suffices to explain β-carotenes photophysics. In other words, S^* does not have to be included as a separate electronic state. For the carotenoid, the S_1-kinetics are still correctly predicted, (Fig. 5(c)), whereas experiment and theory deviate substantially in the region of ESA of S^* (Fig. 5(d)).

4 Discussion

In the current treatment, the theory shows a good agreement with the absorption spectra and most features of the TA spectra for the two studied carotenoid molecules. Our fundamental approach reproduces a number of debated features including the spectral narrowing of ESA associated with the vibrational relaxation within carotenoids. Most remarkably, the displacement between the potential energy surfaces of the two electronic states is shown here to be large enough to produce a vibronic shoulder, once all the excitation has relaxed to the S_1 minimum. In the case of β-carotene (*conf.*, Fig. 3(b) and Fig. 5(b)), this shoulder fully reproduces the spectral features of the earlier postulated S^* state. Furthermore, our model also explains the common finding that the rise-time of S^* is slower than the rise-time of hot-S_1 [17]. For β-carotene, the vibronic model reproduces the experiment in both the S_1 and S^* regions of ESA, indicating that treating vibrational cooling on the S_1 state rigorously is sufficient to fully describe energy relaxation in this molecule.

In the case of the carotenoid sample, however, the kinetic traces taken at the wavelengths corresponding to ESA from S_1 (Fig. 5(c)) and S^* (Fig. 5(d)) show clearly that the present model is correct for S_1, but fails at reproducing S^*-related features. To explain this, we consider previous studies, where a connection between structural inhomogeneity in the electronic ground state and S^* has been drawn [18]. In such an inhomogeneous ground state model (IGSM) [14,20,21], carotenoid photophysics is described by at least two energetically close ground state conformers, both populated at room temperature. S_1 is the lowest lying excited state associated with the global energy minimum S_0. Similarly, S^* is also the lowest lying electronically excited state, but associated with a local minimum on the ground state, S_0^*.

Recently, this model was supported by temperature dependent measurements, showing that S^* is depopulated upon cooling [18]. Additional support for the IGSM comes from the analysis of the GSB signal of carbonyl-containing carotenoids,

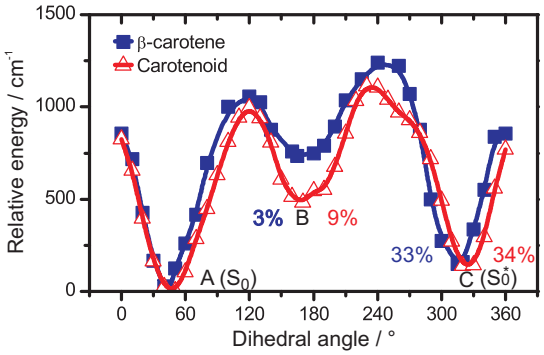

Fig. 6 The electronic B3LYP/def2-SV(P) torsional potentials for the β-ionyliden ring of β-carotene (blue line) and the carotenoid (red line). Conformers are labelled by letters A, B and C, along with their thermal population relative to the global minimum A (S_0) in percent. Conformation C corresponds to the higher-lying local minimum S_0^*.

taken at pump–probe delay times after the depopulation of S_1 but within the lifetime of S^*. Chabera *et al.* showed that the S^*-related GSB signal is narrower and better resolved than the absorption spectrum[37]. This is readily explained within IGSM under the assumption that S_0^* is of higher molecular symmetry than S_0. Indeed, when calculating potential energy surfaces for the rotation of the endgroups for β-carotene, Lukes *et al.* retrieved three minima[21]. The lowest lying global minimum exhibited an asymmetric structure with the endgroups rotated away from the plane of the polyenes. The next higher lying minimum, carrying 33% of the total population at room temperature, showed C_2-symmetry with polyenes and endgroups closer to planarity. In connection with the findings by Chabera *et al.*[37] and the fact that the relative strength of the S^* signal is temperature dependent[18], we assign the symmetric, higher lying minimum to S_0^* and the global minimum to S_0. In support of this hypothesis, a recent study of carotenoids containing aryl endgroups revealed that different dihedral angles between the endgroup and the polyenes lead to different S_1 energies, as well as different $S_1 \rightarrow S_n$ spectra and lifetimes[38].

In IGSM, the ESA signal of the carotenoid consists of two conformation-specific ESA transitions, *i.e.*, $S_1 \rightarrow S_n$ and $S^* \rightarrow S_n^*$, the latter being blue-shifted with respect to the former. To investigate IGSM for the current case, we performed quantum chemical calculations with the aim of locating the possible close-lying ground state conformers upon endgroup rotation. The results are shown in Fig. 6. Using the B3LYP functional, the dihedral angle θ between the plane of the double bonds and one of the endgroups was rotated, while the geometry of the rest of the molecule was optimized for each value of θ. Rotation of the β-ionyliden fragment in β-carotene (blue curve in Fig. 6) reproduces previously published results[21]. We can observe three minima, where the global minimum below 45° (denoted as conformation A) corresponds to S_0, leading to S_1, and the next higher lying local minimum, S_0^*, at 315° (conformation C) is associated with the formation of S^*. The potential for rotation of the aryl end-group, present in the carotenoid sample, is shown in ESI† for comparison, but it is not relevant as a source of inhomogeneity, as two nearly symmetric conformations at 0° and 180° are formed. Conformer C is equally populated at room temperature for both β-carotene (33%) and the carotenoid (34%). In contrast to β-carotene, the carotenoid has an energetically much lower conformation B, with a non-negligible population of 9%. This leads to a larger degree of structural inhomogeneity for the carotenoid in its electronic ground state. The broader line-widths of the excited state spectra of the carotenoid (Fig. 4) along with the stronger S^* signal are hence in support of IGSM.

Yet it is unclear how a minor structural change in the form of rotation of an endgroup accounts for the often largely different electronic lifetimes for S_1 and S^*, *e.g.*, 6.2 ps vs. 9.8 ps in the carotenoid. Given the similarity of the potential curves in Fig. 6 the additional question arises as to why there is a clearly discernible S^* feature in the carotenoid but no need to include S^* for describing dynamics in β-carotene. Recently, Fuciman *et al.* compared two aryl carotenoids with different methylation positions on the aromatic endgroups[38]. Depending on the minimum energy structure, the aromatic endgroups either were a part of the conjugated π-system or were not. If this is the case, the increase in delocalization length lowers the S_1 minimum energy, leading to a decrease of the S_1 lifetime[2]. This connects endgroup rotations to significant changes of delocalization length for the different isomers and has the potential to affect the spectral properties and lifetime of the lowest lying excited state in carotenoids. Hence, this description links IGSM to the dynamic properties, such as the lifetime of the lowest lying electronic state, S_1 or S^*, respectively[18,21]. To prove the connection between endgroup rotation and the energetic position of the lowest lying excited state for the carotenoids in this study, we performed ab initio Multi-Reference Configuration Interaction (MRCI) calculations for isomers A (S_0), B and C (S_0^*) for both β-carotene and the carotenoid. The results are shown in Table 1.

MRCI calculations are computationally expensive (the details of the calculations are presented in ESI†), but were shown to be necessary to reproduce the correct order of states and oscillator strengths of electronic transitions in carotenoids[21,39,40]. The method describes the oscillator strength of transitions to the first and second excited states in agreement with the experimental observation, making S_1 the lowest lying dark excited state and $S_0 \rightarrow S_2$ the first optically allowed transition in all conformers. The transition energies for $S_0 \rightarrow S_2$ are too large when compared with the absorption spectrum in Fig. 1. The values for $S_0 \rightarrow S_1$ need to be reduced when compared to the experimental 0-0 values, as the direct excitation corresponds to the 0-2 excitation[32,41]. Even after

Table 1 The *ab initio* MRCI/RI-def2-SV(P) results for the carotenoid and β-carotene calculated for the B3LYP/def2-SV(P) geometries (conformers A–C, as explained in Fig. 6). The reference space generation started from the three highest occupied molecular orbitals to the four lowest unoccupied molecular orbitals.

	β-carotene		carotenoid	
	E/cm^{-1}	osc. str.	E/cm^{-1}	osc. str.
A	$S_0 \rightarrow S_1$: 19076	0.000	$S_0 \rightarrow S_1$: 12081	0.000
	$S_0 \rightarrow S_2$: 25186	4.096	$S_0 \rightarrow S_2$: 22019	3.765
B	$S_0 \rightarrow S_1$: 20223	0.000	$S_0 \rightarrow S_1$: 8946	0.000
	$S_0 \rightarrow S_2$: 22503	3.771	$S_0 \rightarrow S_2$: 19461	3.519
C	$S_0 \rightarrow S_1$: 19079	0.000	$S_0 \rightarrow S_1$: 13659	0.000
	$S_0 \rightarrow S_2$: 25343	4.038	$S_0 \rightarrow S_2$: 21566	3.786

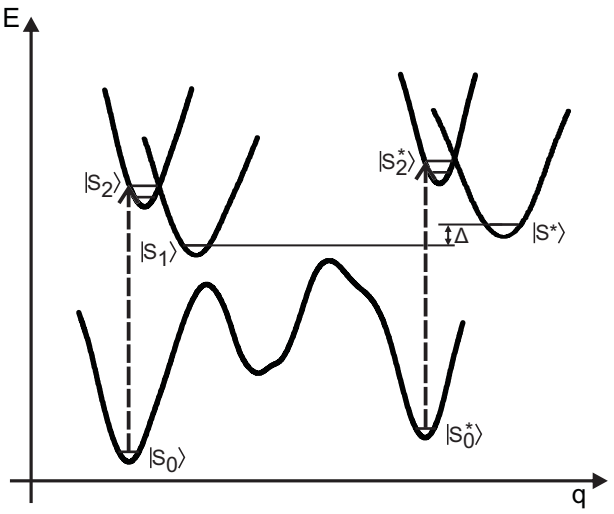

Fig. 7 Sketch of the potential energy surface in IGSM, along with the excited state surfaces for the two main conformers. Excitation (dashed arrows) happens simultaneously for both conformers, as they show indistinguishable absorption spectra. Different lifetimes of S_1 and S^* are explained by a non-zero energy difference Δ, increasing the energy gap between S^* and S_0 along with the lifetime of S^*.

this correction the values are blue-detuned with respect to experimental observations by roughly 2000 cm^{-1}. Despite this discrepancy, which may be avoided by the choice of a larger initial electron reference configuration[42], we find interesting trends when comparing energetic S_1 positions among the two studied molecules. For β-carotene, conformers A (S_0) and C (S_0^*) show nearly identical $S_0 \rightarrow S_1$ transition energies. For the carotenoid on the other hand, S_1 is drastically red-shifted for both conformers. More importantly, conformers A and C now show different $S_0 \rightarrow S_1$ transition energies, with the lowest excited state of the conformer A lying 1578 cm^{-1} beneath that of conformer C. This readily explains the observed lifetime differences within IGSM. Given that the internal conversion between S_0 and S_1 closely follows the energy gap law[2,32], the state with the smaller energy gap to S_0 relaxes more rapidly. For β-carotene, both S_1 and S^* will decay on indistinguishable time-scales, considering their almost identical energy gap with respect to S_0. Hence, we excite a mixture of two conformers A and C, which then decay on roughly the same effective time-scale. For the carotenoid, on the other hand, the two major conformers give two lowest lying excited states with appreciably different energy gaps to their respective ground states. We note that the DFT-based calculations estimate the conversion between conformers A and C to happen on nanosecond time-scales[21] and can be excluded for the purposes of this study. This means that the two isomers predicted by IGSM are observable in the carotenoid based on the larger energy difference, Δ, between their respective first excited states, which is not the case for β-carotene, where Δ is too small for isomer-specific time-scales beyond experimental error. This scenario is summarized in Figure 7.

Interestingly, for the carotenoid we find a broad, low-intensity tail on the red edge of the absorption spectum, which is missing for β-carotene (*conf.*, Fig. 1). We can attribute this tail to the absorption of the B conformer of the carotenoid, which possesses the lowest $S_0 \rightarrow S_2$ transition energy according to Table 1. The fact that conformer B has lower B3LYP/def2-SV(P) relative energy in the carotenoid than in β-carotene (9% vs. 3% of total population in B, see Fig. 6) serves as a straight forward explanation of the observed differences in the red edge of the linear absorption. Moreover, absorption spectra of β-carotene at high temperature showed an additional absorption peak, red-shifted to the main transition[8]. This finding is readily explained by conformer B gaining higher population density upon heating.

In addition to the present work, IGSM simultaneously explains the temperature dependent S_1-to-S^* signal ratio[16,18] and several other experimental findings, such as the pump–deplete–probe[11], spectral changes of GSB signal with delay time[37], and temperature-dependent absorption measurements[8].

5 Experimental

Sample preparation

β-carotene was purchased from Sigma-Aldrich and dissolved in spectroscopic grade benzonitrile. The carotenoid was synthesized according to published procedures[30] and dissolved in spectroscopic grade toluene. The solvents used for the two investigated molecules show different polarizability, ensuring similar absorption spectra as depicted in Fig. 1. Optical densities in the visible spectral range were kept below 0.3 OD for

both samples for a path-length of 0.5 mm. The sample was exchanged fully between two laser shots.

TA experiment

The experimental details were published previously[43,44]. Briefly, an amplified Ti:Sapphire laser system (Clark CPA-2001), operated at 1 kHz, pumped a non-collinear optical parametric amplifier system, producing the near-transform limited pulses (18 fs) with a spectrum depicted in Fig. 1. Excitation pulse energies were set to 100 nJ or 5×10^{14} photons cm^{-2}. For probing, a small, adjustable fraction of the fundamental light was focused into either a 2 mm thick sapphire plate (carotenoid) or a rotating CaF_2-disc (β-carotene). To avoid anisotropy related effects, the polarization angle between pump- and probe-pulses was set to the magic angle of 54.7°.

6 Conclusions

Simulation of the experimental data within a quantum mechanical model helps us understand the nature of S^* feature in two different carotenoids. We agree with Holzwarth and coworkers[19] that one can describe the photodynamics of β-carotene by vibrational cooling, and that S^* as a separate electronic state is not necessary. In the case of the investigated carotenoid, vibrational cooling cannot reproduce all the experimentally observed spectral components, even when using large potential curve displacements. In fact, any carotenoid with a large lifetime difference between $S^*$and S_1, which may amount to several picoseconds in long-chain carotenoids[4], will present the same interpretational difficulty. In such cases, we propose that the structural inhomogeneity in the ground state serves as an explanation for S^*, viewing it as the lowest lying electronically excited state derived from a local ground state minimum; the S^* feature is then nothing but the S_1 signal of a different thermally populated ground state. Essentially, we consider two sub-species of carotenoid configurations: the one with states S_0, S_1, S_2, S_n, and the other with states S_0^*, S^*, S_2^*, S_n^*. Populations of these conformational isomers are necessarily determined by the energy difference between S_0 and S_0^*, while the energy gaps between the lowest lying excited state and the ground state determine their depopulation times. As for the scope of VERA, it is readily extended to any internal conversion process in large organic molecules, where vibrational modes are plenty and which mediate the electronic relaxation process. We therefore put our method forward as a new alternative in interpreting the relaxation processes in such systems. The method is particularly suited for analysing TA data as it circumvents several shortcomings related to data fitting by GTA.

Acknowledgments

D.A. and V. B. acknowledge the support of the Research Council of Lithuania (LMT grant no. MIP-090/2015). A. G. P, C. L. and J. H. acknowledge funding by the Austrian Science Fund (FWF): START project Y 631-N27. We thank Prof. Ana Moore for supplying us with the carotenoid sample and Dr. Igor Pugliesi for experimental help.

References

1 M. Klessinger and J. Michl, *Excited States and Photochemistry of Organic Molecules*, VCH Publ., New York, 1995.
2 T. Polívka and V. Sunström, *Chem. Rev.*, 2004, **104**, 2021–2071.
3 C. C. Gradinaru, J. T. M. Kennis, E. Papagiannakis, I. H. M. van Stokkum, R. J. Cogdell, G. R. Fleming, R. A. Niederman and R. van Grondelle, *Proc. Nat. Acad. Sci. USA*, 2001, **98**, 2364–2369.
4 T. Polívka and V. Sunström, *Chem. Phys. Lett.*, 2009, **477**, 1–11.
5 E. Papagiannakis, J. T. M. Kennis, I. H. M. van Stokkum, R. J. Cogdell and R. van Grondelle, *Proc. Nat. Acad. Sci. USA*, 2002, **99**, 6017–6022.
6 D. Kosumi, S. Maruta, T. Horibe, Y. Nagaoka, R. Fujii, M. Sugisaki, R. J. Cogdell and H. Hashimoto, *J. Chem. Phys.*, 2012, **137**, 064505.
7 M. Kloz, S. Pillai, G. Kodis, D. Gust, T. A. Moore, A. L. Moore, R. van Grondelle and J. T. M. Kennis, *Chem. Sci.*, 2012, 2052.
8 T. Lenzer, F. Ehlers, M. Scholz, R. Oswald and K. Oum, *Phys. Chem. Chem. Phys.*, 2010, **12**, 8832–8839.
9 T. Buckup, J. Savolainen, W. Wohlleben, J. L. Herek, H. Hashimoto, R. R. B. Correia and M. Motzkus, *J. Chem. Phys.*, 2006, **125**, 194505.
10 P. O. Andersson and T. Gilbro, *J. Chem. Phys.*, 1995, **103**, 2509–2519.
11 J. Savolainen, T. Buckup, J. Hauer, A. Jafarpour, C. Serrat, M. Motzkus and J. L. Herek, *Chem. Phys.*, 2009, **357**, 181–187.
12 K. Golibrzuch, F. Ehlers, M. Scholz, R. Oswald, T. Lenzer, K. Oum, H. Kim and S. Koo, *Phys. Chem. Chem. Phys.*, 2011, **13**, 6340–6351.
13 A. E. Jailaubekov, S. H. Song, M. Vengris, R. J. Cogdell and D. S. Larsen, *Chem. Phys. Lett.*, 2010, **487**, 101–107.
14 N. Christensson, F. Milota, A. Nemeth, J. Sperling, H. F. Kauffmann, T. Pullerits and J. Hauer, *J. Phys. Chem. B*, 2009, **113**, 16409–16419.
15 D. M. Niedzwiedzki, J. O. Sullivan, T. Polvka, R. R. Birge and H. A. Frank, *J. Phys. Chem. B*, 2006, **110**, 22872–22885.
16 D. Niedzwiedzki, J. F. Koscielecki, H. Cong, J. O. Sullivan, G. N. Gibson, R. R. Birge and H. A. Frank, *J. Phys. Chem. B*, 2007, **111**, 5984–5998.
17 A. E. Jailaubekov, M. Vengris, S.-H. Song, T. Kusumoto, H. Hashimoto and D. S. Larsen, *J. Phys. Chem. A*, 2011, **115**, 3905–3916.
18 J. Hauer, M. Maiuri, D. Viola, V. Lukes, S. Henry, A. M. Carey, R. J. Codgell, G. Cerullo and D. Polli, *J. Phys. Chem. A*, 2013, **117**, 6303–6310.
19 E. E. Ostroumov, M. G. Müller, M. Reus and A. R. Holzwarth, *J. Phys. Chem. A*, 2011, **115**, 3698–3712.
20 E. Papagiannakis, I. H. M. van Stokkum, M. Vengris, R. J. Codgell, R. van Grondelle and D. S. Larsen, *J. Phys. Chem. B*, 2006, **110**, 5727–5736.
21 V. Lukes, N. Christensson, F. Milota, H. Kauffmann and J. Hauer, *Chem. Phys. Lett.*, 2011, **506**, 122–127.
22 A. Holzwarth, *Biophysical Techniques in Photosynthesis*, 1996, pp. 75–92.
23 I. H. M. van Stokkum, D. S. Larsen and R. van Grondelle, *Biochim. Biophys. Acta*, 2004, **1657**, 82–104.
24 H. Marciniak and S. Lochbrunner, *Chemical Physics Letters*, 2014, **609**, 184–188.
25 L. Valkunas, D. Abramavicius and T. Mančal, *Molecular Excitation Dynamics and Relaxation*, Wiley-VCH, Weinheim, 2013.

26 V. May and O. Kühn, *Charge and Energy Transfer in Molecular Systems*, Wiley-VCH Verlag GmbH, Weinheim, 2004.

27 D. Polli, G. Cerullo, G. Lanzani, S. De Silvestri, H. Hashimoto and R. J. Codgell, *Biophys. J.*, 2006, **90**, 2486–2497.

28 T. Buckup, J. Hauer, J. Möhring and M. Motzkus, *Arch. Biochem. Biophys*, 2009, **483**, 219–223.

29 J. P. Kraack, A. Wand, T. Buckup, M. Motzkus and S. Ruhman, *Phys. Chem. Chem. Phys.*, 2013, **15**, 14487–14501.

30 A. N. Macpherson, P. A. Liddell, D. Kuciauskas, D. Tatman, T. Gillbro, D. Gust, T. A. Moore and A. L. Moore, *J. Phys. Chem. B*, 2002, **106**, 9424–9433.

31 N. Christensson, F. Milota, A. Nemeth, I. Pugliesi, E. Riedle, J. Sperling, T. o. Pullerits, H. F. Kauffmann and J. Hauer, *J. Phys. Chem. Lett.*, 2010, **1**, 3366–3377.

32 D. Kosumi, M. Fujiwara, R. Fujii, R. J. Codgell, H. Hashimoto and M. Yoshizawa, *J. Chem. Phys.*, 2009, **130**, 214506.

33 F. L. de Weerd, I. H. M. van Stokkum and R. van Grondelle, *Chem. Phys. Lett.*, 2002, **354**, 38–43.

34 H. H. Billsten, D. Zigmantas, V. Sunström and T. Polívka, *Chem. Phys. Lett.*, 2002, **355**, 465–470.

35 F. D. Fuller, J. Pan, A. Gelzinis, V. Butkus, S. S. Senlik, D. E. Wilcox, C. F. Yocum, L. Valkunas, D. Abramavicius and J. P. Ogilvie, *Nature Chem.*, 2014, **6**, 706–711.

36 E. Romero, R. Augulis, V. I. Novoderezhkin, M. Ferretti, J. Thieme, D. Zigmantas and R. van Grondelle, *Nat Phys*, 2014, **10**, 676–682.

37 P. Chabera, M. Fuciman, P. Hribek and T. Polivka, *Physical Chemistry Chemical Physics*, 2009, **11**, 8795–8803.

38 M. Fuciman, G. Kesan, A. M. LaFountain, H. A. Frank and T. Polívka, *J. Phys. Chem. B*, 2015, **119**, 1457–1467.

39 S. Grimme and M. Waletzke, *J. Chem. Phys.*, 1999, **111**, 5645.

40 M. Kleinschmidt, C. Marian, M. Waletzke and S. Grimme, *J. Chem. Phys.*, 2009, **130**, 044708.

41 R. L. Christensen, M. Goyette, L. Gallagher, J. Duncan and B. DeCoster, *J. Phys. Chem. A*, 1999, **103**, 2399–2407.

42 M. R. Silva-Junior, M. Schreiber, S. P. Sauer and W. Thiel, *J. Chem. Phys.*, 2008, **129**, 104103.

43 J. Savolainen, N. Dijkhuizen, R. Fanciulli, P. A. Liddell, D. Gust, T. A. Moore, A. L. Moore, J. Hauer, T. Buckup, M. Motzkus and J. L. Herek, *J. Phys. Chem. B*, 2008, **112**, 2678–2685.

44 U. Megerle, I. Pugliesi, C. Schriever, C. Sailer and E. Riedle, *Applied Physics B*, 2009, **96**, 215–231.